THE ASTROPHYSICAL JOURNAL, 530:429–440, 2000 February 10

THE 0.1–100 keV SPECTRUM OF CENTAURUS X-3: PULSE PHASE SPECTROSCOPY OF THE CYCLOTRON LINE AND MAGNETIC FIELD STRUCTURE

L. BURDERI,[1] T. DI SALVO,[1] N. R. ROBBA,[1] A. LA BARBERA,[1] AND M. GUAINAZZI[2]
Received 1999 February 19; accepted 1999 September 29

ABSTRACT

We report spectral and temporal analysis of the X-ray pulsar Centaurus X-3 out of eclipse observed by *BeppoSAX*. The broadband spectrum (0.12–100 keV) is well described by an absorbed power law modified by a high-energy rollover at $\sim$14 keV (*e*-folding energy $\sim$8 keV) plus an iron emission line at $\sim$6.7 keV. A soft excess below 1 keV is also present. Interpreted as a blackbody ($kT \simeq 0.1$ keV), it corresponds to 58% of the total unabsorbed flux. This component seems to originate from reprocessing of the primary radiation by an opaque shell located at the magnetosphere. An absorption feature at $\sim$30 keV is also present. Interpreted as a cyclotron line, after correction for gravitational redshift, this corresponds to a surface magnetic field of $\sim 3.5 \times 10^{12}$ G. Phase-resolved spectroscopy reveals a variation by about 8 keV of the cyclotron resonance energy along the pulse profile. In particular, the line energy decreases from $\sim$36 to $\sim$28 keV along the peak, starting from the ascent. The asymmetric variations of the cyclotron line energy can be explained by assuming an offset of the dipolar magnetic field with respect to the neutron star center. The spectral results are discussed in terms of emission from magnetic caps, where Comptonization of soft photons occurs. The soft photons could come from either magnetically resonant double Compton scattering or from illumination of the polar cap by the primary radiation reprocessed at the magnetospheric surface, a feedback mechanism similar to that proposed for the formation of black hole spectra.

Subject headings: stars: individual (Centaurus X-3) — stars: magnetic fields — stars: neutron — X-rays: stars

1. INTRODUCTION

The X-ray source Centaurus X-3 is a high-mass X-ray binary with a spin period of $\sim$4.8 s and an orbital period of $\sim$2.1 days (see Nagase 1989 for a review). Spectroscopic observations in the optical band allowed the determination of the orbital parameters and indicate that the companion is an O6–O8 type supergiant (V779 Cen) of radius $R_c \sim 12$ $R_\odot$ and mass $M_c \sim 17$–19 $M_\odot$ (Hutchings et al. 1979). The distance of the system is estimated to be $\sim$8 kpc (Krzemiński 1974). The X-ray data show eclipses for $\sim$20% of the orbit (see Nagase 1989). The intensity of this source is variable: adopting a distance of 8 kpc, the *Ginga* 1989 data showed that the luminosity of this source was 5×10^{37} ergs s^{-1} (Nagase et al. 1992), which is about half of the previously observed average luminosity (White, Swank, & Holt 1983). The Broad Band X-Ray Telescope (BBXRT) 1990 observation (Audley et al. 1996) has shown an increase of the luminosity by a factor of $\sim$1.4 with respect to the previous *Ginga* (1989) observation. In general, variations of up to a factor of 8 between "high" and "low" states have been observed. Priedhorsky & Terrell (1983) found that this behavior has a characteristic timescale of 120–165 days, although they found no evidence for periodicity.

The time variability of this source is one of the most complex among the massive X-ray binaries. The spin period has been monitored by various X-ray missions over the past 20 yr, revealing a trend of secular spin-up of $\dot{P} = -1.135$ ms yr^{-1}, with wavy fluctuations on a timescale of few years (see, e.g., Hiroshi, Kitamoto, & Tamura 1996). Among the massive X-ray binaries, only a few show variations in the orbital period. Cen X-3 shows a secular decay of the orbital period, probably due to tidal dissipation. The orbital ephemeris has recently been improved by Nagase et al. (1992). The pulse profile is also variable in shape. At high energies (roughly above 10 keV) the pulse profile is clearly single-peaked. At lower energy its shape is more complex and variable, although several authors (e.g. Van der Klis, Bonnet-Bidaud, & Robba 1980; White et al. 1983) have reported a single-peaked structure in the range 1–50 keV. A more recent *Ginga* observation has shown a double-peaked structure in the 1–10 keV range (Nagase et al. 1992).

The 1–40 keV X-ray spectrum has been fitted by a power law with a high-energy cutoff, iron line, and soft X-ray absorption (White et al. 1983). The analysis of *Ginga* data by Nagase et al. (1992) showed that the high-energy cutoff is better modeled by a quasi-Lorentzian high-energy turnover resembling the effects of a cyclotron resonant scattering, rather than by the usual *e*-folding energy cutoff, although their fit does not provide firm evidence of the cyclotron resonant scattering, because the energy of the line ($\sim$30 keV) is very close to the upper end of the *Ginga* LAC detectors. The presence of a cyclotron line at $\sim$30 keV has been confirmed by Santangelo et al. (1998). The emission feature at $\sim$6.6 keV detected by Nagase et al. (1992) has been fitted with two lines at the fixed energies of 6.4 and 6.7 keV, the former arising from iron fluorescence from cold matter, the latter arising from hot, helium-like iron ions. Based on an analysis of data during the eclipse, the size of this ionized region is $\geq 8 \times 10^{11}$ cm. On the other hand, the abrupt eclipse of the 6.4 keV line indicates that this line originates from reprocessing by matter orbiting around the neutron star in an accretion disk. The size of this emitting region is $\leq 3 \times 10^8$ cm. The luminosities of these lines during the

[1] Dipartimento di Scienze Fisiche ed Astronomiche, Università di Palermo, via Archirafi 36-90123 Palermo, Italy; burderi@gifco.fisica.unipa.it.
[2] Space Science Department of ESA, ESTEC/SA, Postbus 299-2200 AG Noordwijk, The Netherlands.

high-luminosity post-eclipse phase are $L_{6.4} \sim 5 \times 10^{35}$ and $L_{6.7} \sim 1 \times 10^{35}$ ergs s^{-1}, respectively (Nagase et al. 1992).

In this paper we report temporal and broadband (0.1–100 keV) spectral analysis of Cen X-3 out of eclipse based on an observation performed by the *BeppoSAX* narrow-field instruments. We also analyzed *ASCA* and *ROSAT* data of Cen X-3 out of eclipse. The results of this analysis are in line with the *BeppoSAX* results.

2. OBSERVATIONS

BeppoSAX observed Cen X-3 with its narrow-field instruments (NFI; Boella et al. 1997a) from 1997 February 27 19:45 to February 28 11:00 (UT), covering the phase interval 0.0–0.28 of the 2.1 day orbital period (phase 0.0 is mid-eclipse).

The spectral coverage of *BeppoSAX*, extending over more than three decades of energy (from 0.1 up to 200 keV), is provided by four coaligned instruments: the Low-Energy Concentrator Spectrometer (LECS), operating in the energy range 0.1–10 keV (Parmar et al. 1997); the Medium-Energy Concentrator Spectrometer (MECS), consisting of three units operating in the range 1–10 keV (Boella et al. 1997b); the High-Pressure Gas Scintillation Proportional Counter (HPGSPC), operating in the range 4–120 keV (Manzo et al. 1997); and the Phoswich Detector System (PDS), with four scintillation units operating in the range 15–300 keV (Frontera et al. 1997). All the instruments have approximately 1° fields of view (FOV). LECS and MECS have imaging capabilities; therefore, we extracted the data from circular regions in the LECS and MECS FOVs of 8′ and 4′, respectively, centered on the maximum of the point-spread function (PSF). The background subtraction is obtained using blank-sky observations and extracting the background spectra from a circular region corresponding to the one used for the source. The HPGSPC and PDS spectra do not have imaging capabilities, and the subtraction of the background is obtained using off-source data resulting from the rocking of the collimators.

Figure 1 shows the Cen X-3 light curve, binned at 107 s, in two different energy bands: 1–10 keV (MECS data, *top*) and 15–100 keV (PDS data, *bottom*). This light curve shows the source in its eclipse state during the first 15 ks and out of eclipse in the last 30 ks.

The post-egress flux is 5.7×10^{-9} ergs cm^{-2} s^{-1} in the 2–10 keV energy band and 1.3×10^{-8} ergs cm^{-2} s^{-1} in the 0.12–100 keV band. Adopting a distance of 8 kpc (Krzemiński 1974), the source luminosity is $\sim 4.4 \times 10^{37}$ ergs s^{-1} in the energy range 2–10 keV and $\sim 1.0 \times 10^{38}$ ergs s^{-1} in the whole range 0.12–100 keV. Following common practice, we have not included any gravitational correction to the reported luminosities.

In this paper we concentrate our analysis on data out of eclipse. The exposure time during the post-egress phase is ~ 2 ks in the LECS (because it was not active for most of the observation), ~ 21 ks in the MECS, ~ 11 ks in the HPGSPC, and ~ 8 ks in the PDS.

3. TEMPORAL ANALYSIS

Because of the better statistics, we used MECS data to perform a temporal analysis. The arrival times of all the events were reported to the solar system barycenter. We divided the whole data set into 19 consecutive intervals of ~ 1640 s each. A folding search around the period reported in the literature was performed in each interval. The corre-

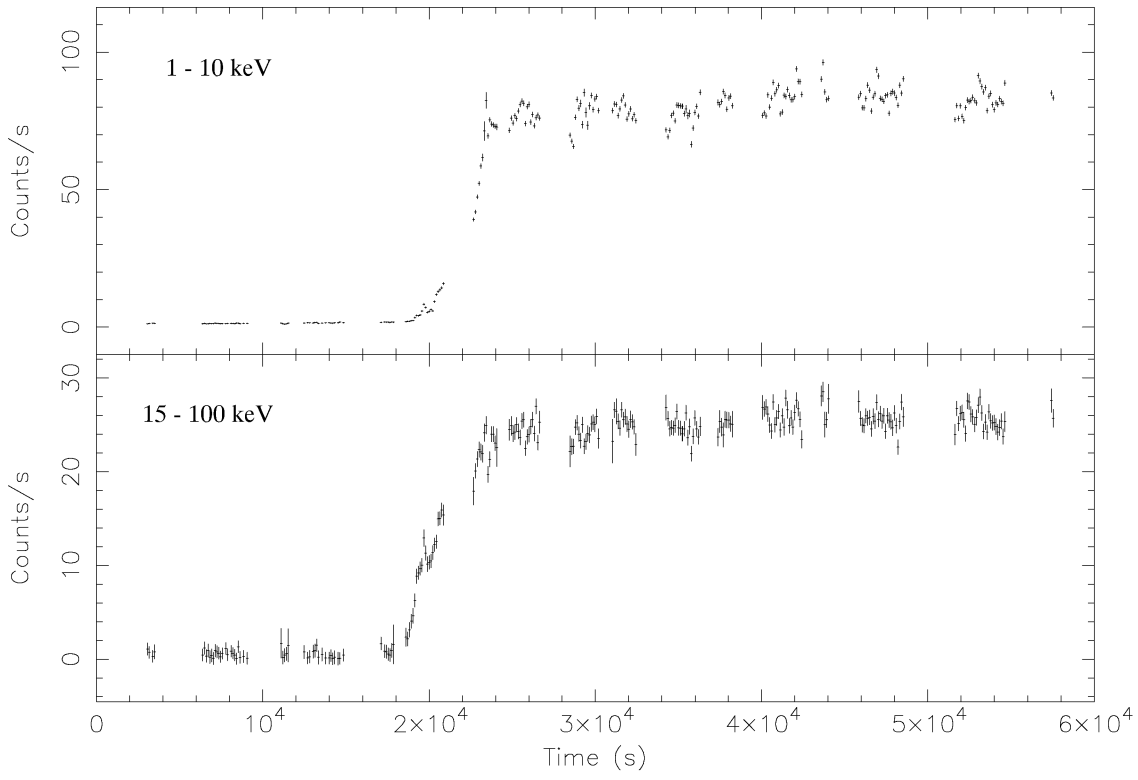

FIG. 1.—Light curve binned at 107 s of the whole *BeppoSAX* observation of Cen X-3. *Top*: MECS data (1–10 keV). *Bottom*: PDS data (15–100 keV).

sponding best periods were obtained by fitting the χ^2 versus trial period curve with a Gaussian. The Doppler effect on the spin period induced by the orbital motion was clearly visible, although the time interval is too short to constrain the orbital period. We fitted these periods with the function

$$P(t) = P_0 + A \sin\left[\frac{2\pi(t - T_0)}{P_{\rm orb}}\right],$$

fixing the orbital period $P_{\rm orb}$ to the value of 2.08704363 days, calculated from the ephemeris reported by Nagase et al. (1992), taking into account the orbital-period derivative. From the fit we obtained the intrinsic pulse period $P_0 = 4.8146 \pm 0.0005$ s and the mid-eclipse time $T_0 = 50506.776 \pm 0.007$ MJD, consistent, within errors, with the value calculated from Nagase et al. (1992). Using these ephemeris, we corrected the arrival times of all the events for the orbital modulation. Then we performed a folding search for the best period on these corrected arrival times. The best period obtained was 4.81423 ± 0.00001 s, demonstrating that the source is still in a spin-up state.

Figure 2 shows the pulse profiles during the post-egress phase in different energy bands, namely, 0.1–1.8 keV (Fig. 2*a*), 1.8–10.5 keV (Fig. 2*b*), and 15–60 keV (Fig. 2*c*). A small interpulse is evident in the soft energy range, progressively disappearing at higher energies. We folded the MECS data modulo the spin period in the energy intervals 1–4 keV and 4–11 keV and computed the hardness ratio (4–11) keV/(1–4) keV (Fig. 2*d*). This ratio confirms that the interpulse is softer than the main pulse.

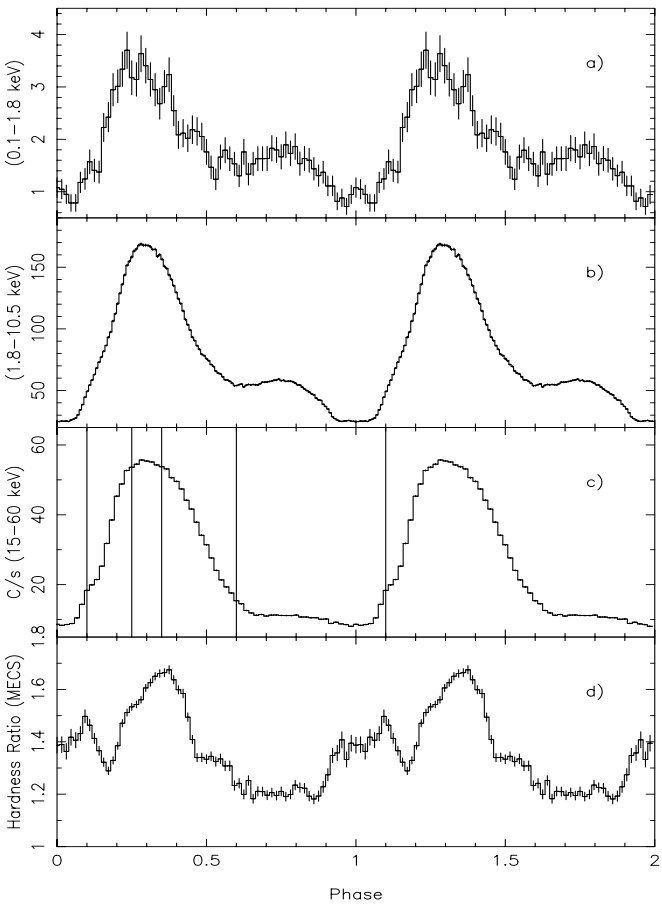

FIG. 2.—(*a*) Cen X-3 pulse profile in the energy range 0.1–1.8 keV. (*b*) Same as (*a*), in the energy range 1.8–10.5 keV. (*c*) Same as (*a*), in the energy range 15–60 keV. The four phase intervals used to extract the pulse-phase–resolved spectra are also shown. (*d*) Hardness ratio 4–11 keV/1–4 keV.

4. PULSE-PHASE–AVERAGED SPECTRUM

Spectral analysis was performed on the post-egress energy spectrum of Cen X-3 in the energy range 0.12–100 keV. The energy ranges used for each NFI are: 0.12–4 keV for LECS, 1.8–10 keV for MECS, 10–20 keV for HPGSPC, and 15–100 keV for PDS. Different normalizing factors for the four instruments were included, fixed to 1 for the MECS and kept free for the other instruments.

Following the results of Nagase et al. (1992), we tried to fit the spectrum with an absorbed power-law modified by an absorption cyclotron line of quasi-Lorentzian shape (Mihara 1995) plus a Gaussian iron emission line at ~ 6.4 keV. This model gave an unacceptable fit, with a reduced χ^2 of 2.8. In particular, the high-energy part of the spectrum (above ~ 10 keV) is not well fitted by an absorption feature alone (as in the analysis of *Ginga* data by Nagase et al. 1992). The broader band of the *BeppoSAX* instruments unambiguously demonstrate that both an absorption feature and an exponential cutoff are needed to adequately model the spectrum. Indeed, we obtained a very good fit (reduced $\chi^2 = 1.0$) by adopting a power law with a high-energy cutoff, smoothed around the cutoff energy, given by

$$S(E) = \begin{cases} NE^{-\alpha} & \text{for } E \le E_{\rm cut} - \Delta E\,, \\ c_3 E^3 + c_2 E^2 + c_1 E + c_0 & \\ \qquad \text{for } E_{\rm cut} - \Delta E < E < E_{\rm cut} + \Delta E\,, & (1) \\ NE^{-\alpha} \exp\left[-(E - E_{\rm cut})/E_{\rm fold}\right] & \\ \qquad \text{for } E \ge E_{\rm cut} + \Delta E\,, \end{cases}$$

modified at low energies for absorption by cold matter and multiplied by an absorption cyclotron line of Gaussian shape, plus a blackbody to model a soft excess and a Gaussian to fit an iron emission line. The constants c_0, c_1, c_2, and c_3 were calculated assuming the continuity of the function $S(E)$ and its derivatives in $E_{\rm cut} - \Delta E$ and $E_{\rm cut} + \Delta E$, respectively, where the width ΔE is a free parameter of the fit.

The best-fit parameters are shown in Table 1, and the observed spectrum and the residuals are shown in Figure 3 (*top and middle panels, respectively*). The best-fit spectral model is shown in Figure 4.

The function $S(E)$ that we adopted to fit the continuum is a modified version of the widely used "power law with high-energy cutoff," defined by

$$H(E) = \begin{cases} NE^{-\alpha} & \text{for } E \le E_{\rm cut}\,, \\ NE^{-\alpha} \times \exp\left[-(E - E_{\rm cut})/E_{\rm fold}\right] & \text{for } E > E_{\rm cut}\,. \end{cases}$$

$H(E)$ has a cusp (discontinuous derivative) in $E = E_{\rm cut}$. Using $H(E)$ instead of $S(E)$, we still found an acceptable fit (reduced $\chi^2 = 1.2$), but the residuals showed a wedge-shaped feature around 15 keV (see Fig. 3, *bottom*), where $H(E)$ has its cusp. Because a cusp in the continuum has no physical meaning, we believe that $H(E)$ has been extensively used in the past because its simple analytical form was adequate for data of moderate statistical quality. However, as the statistical significance of the data around the cutoff region has improved (thanks to the present generation of X-ray satellites), the use of $H(E)$ generates features that could even mimic absorption lines at the cutoff energy. This

TABLE 1

RESULTS OF THE FIT IN THE ENERGY RANGE 0.1–100 keV

Parameter	Value
N_H	$(1.95 \pm 0.03) \times 10^{22}$ cm^{-2}
kT_{BB}	0.110 ± 0.012 keV
Blackbody normalization	$0.26^{+0.29}_{-0.13}$
Photon index	1.208 ± 0.007
Smoothing width	3.1 ± 0.3 keV
Normalization	0.708 ± 0.008
E_{cut}	13.79 ± 0.13 keV
E_{fold}	8.39 ± 0.19 keV
E_{Fe}	6.666 ± 0.025 keV
σ_{Fe}	0.302 ± 0.035 keV
I_{Fe}	$(7.7 \pm 0.5) \times 10^{-3}$ photons cm^{-2} s^{-1}
Fe equivalent width	107 eV
E_{cyc}	30.6 ± 0.6 keV
σ_{cyc}	5.9 ± 0.7 keV
Eye equivalent width	11.4 ± 2.0 keV
χ^2/dof	651/646

NOTE.—Uncertainties are at the 90% confidence level for a single parameter. Power-law normalization is in units of 10^{-2} photons keV^{-1} cm^{-2} s^{-1} at 1 keV. Blackbody normalization is the flux in units of 10^{39} ergs for a distance of 10 kpc.

is shown in Figure 5, where we plot $S(E)$, $H(E)$, and their difference around the cusp.

We found an iron emission line at 6.67 keV with an equivalent width of 107 eV and intrinsic width of 0.3 keV.

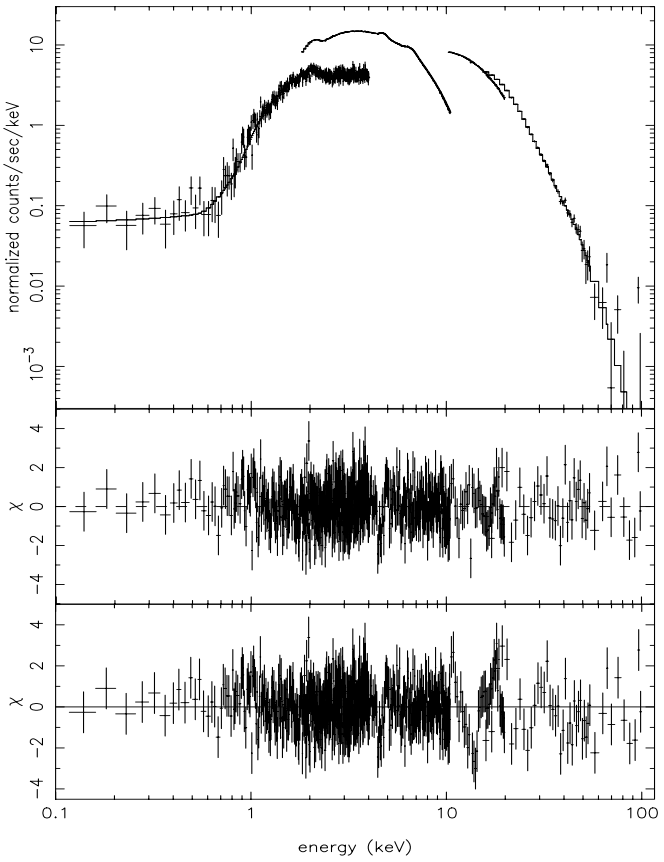

FIG. 3.—*Top*: Pulse-averaged spectrum of Cen X-3 in the whole energy range of *BeppoSAX* (0.1–100 keV). *Middle*: Residuals in units of σ with respect to the best-fit model containing the smoothing around the cutoff energy (see text). *Bottom*: Residuals in units of σ with respect to the model not containing the smoothing. In this case, a feature in the residuals is visible at the cutoff energy (14 keV).

To test the hypothesis that this line results from a blending of lines corresponding to different ionization states, as previously suggested by some authors (e.g. Nagase et al. 1992), we tried to fit the spectrum using two lines at fixed energies of 6.4 and 6.7 keV, respectively. This modification did not improve the fit, although the MECS does not have enough energy resolution to exclude line blending.

5. PULSE-PHASE–RESOLVED SPECTRAL ANALYSIS

To investigate the dependence of the cyclotron line parameters on pulse phase, we extracted phase-resolved spectra in the energy interval 1.8–100 keV according to the four phase intervals: *ascent* (phases 0.1–0.25), *maximum* (0.25–0.35), *descent* (0.35–0.6), and *minimum* (0.6–1.1), shown in Figure 2*c*. The LECS data (0.12–4 keV) were excluded because of their low statistics. The four spectra were fitted with the same model used for the whole data set. The results are shown in Table 2. The detection of the cyclotron line was not statistically significant in the phase interval 0.6–1.1, corresponding to the minimum of the pulse profile. In this case, we fixed the energy and the width of the line to the values obtained for the pulse-averaged spectrum to derive an upper limit on the equivalent width. This upper limit (8 keV) is comparable to the averaged equivalent width of the cyclotron line. On the other hand, we clearly detected the line in the remaining phase intervals. The centroid of the line shows a strong asymmetric dependence on the pulse phase, having its maximum in the ascent and decreasing along the pulse profile. To show the variations of the cyclotron line along the pulse profile, in Figure 6 we plot the ratio $R = F_{data}(E)/S_{fit}(E)$ in various phase intervals, where $F_{data}(E)$ is the total flux, as derived from the data, and $S_{fit}(E)$ is the continuum defined by equation (1) (that does not include the cyclotron line) as derived from the best fit.

6. COMPARISON WITH PREVIOUS *ASCA* AND *ROSAT* OBSERVATIONS

We have also analyzed archival *ASCA* and *ROSAT* pointed observations of Cen X-3, in order to compare the *BeppoSAX* measure of the soft X-ray thermal component with the results obtained by other satellites. The *ASCA* payload (Tanaka, Inoue, & Holt 1994; Makishima et al. 1996) nominally covers the energy band between 0.5 and 10 keV with a pair of charge-couple devices (the Solid Imaging Spectrometers, SIS0 and SIS1) and a pair of gas scintillating proportional counters (Gas Imaging Spectrometers, GIS2 and GIS3). The main differences from *BeppoSAX* are a $\simeq 2$ higher total effective area in the intermediate (i.e. 1–10 keV) X-rays and a much better energy resolution ($\simeq 2\%$ at 6 keV, slowly degrading with time) provided by the SIS. On the other hand, the *ROSAT* PSPC nominally covers the energy band 0.1–2 keV, with energy resolution comparable to that of the LECS, but an effective area about 1 order of magnitude higher (although sharply decreasing around the carbon edge).

ASCA observed Cen X-3 from 1995 February 1 12:39:53 to February 2 16:00:07 (UTC). We analyze data corresponding to orbital phases between 0.50 and 0.83. Source spectra have been extracted from circular regions of 4′, 3.′25, and 6′ around the centroid of the source for the SIS0, SIS1, and GIS, respectively. Background spectra have been standardly extracted from blank-sky fields in the same extraction region and detector coordinates as the source in the

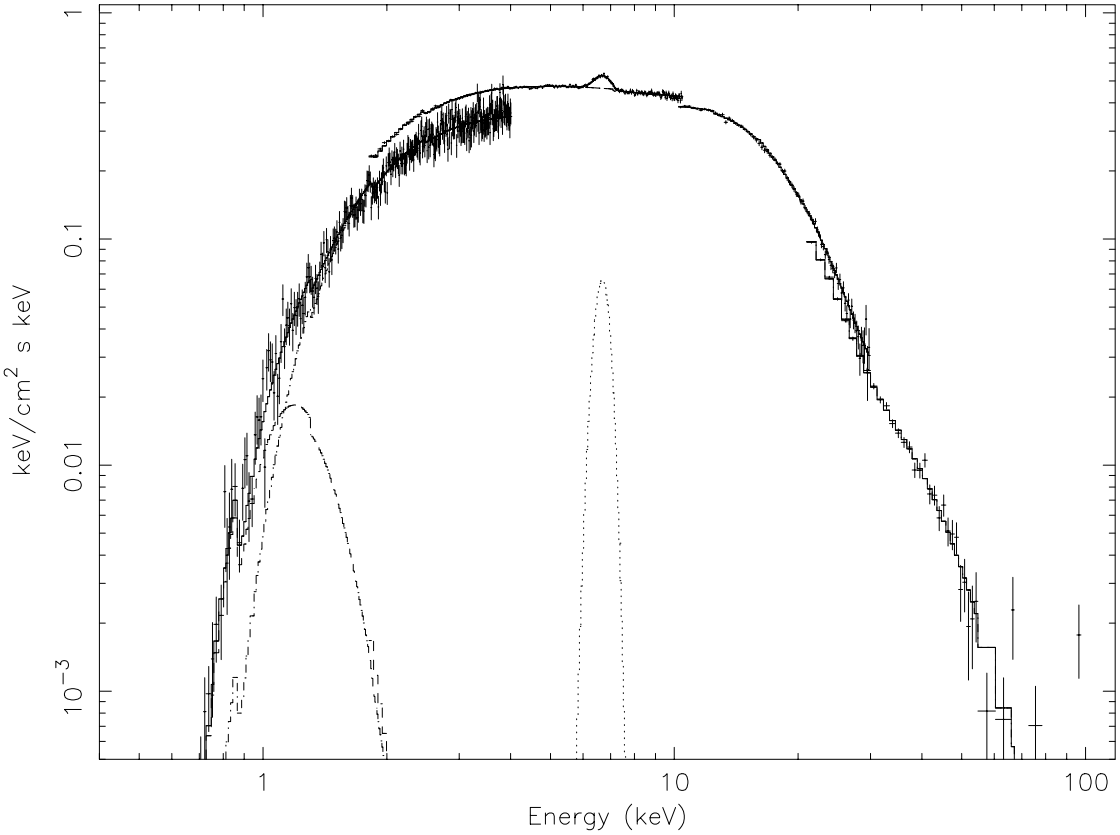

FIG. 4.—Deconvolved pulse-averaged spectrum of Cen X-3. The single components, namely, the power law with exponential cutoff multiplied by the cyclotron absorption line, the blackbody at ~ 0.1 keV, and the Gaussian iron line at ~ 6.7 keV, are also shown.

SIS, and from circular, source-photon–free regions of the field of view in the GIS. The spectra of all the instruments have been fitted simultaneously, using the energy bands 0.5–9 keV and 0.7–10 keV for the SIS and the GIS, respectively. Constant factors have been multiplied to all the models discussed below to account for the residual absolute flux miscalibration between the *ASCA* detectors and a possible unequal sampling of the strongly variable out-of-eclipse flux (we remind the reader that the data-screening criteria are different among the instruments). We have first tried a continuum constituted by a power-law, because the exponential cutoff is out of the range of the *ASCA* detectors, plus a system of fluorescent iron emission lines, corresponding to various ionization stages. The quality of the fit is marginally acceptable ($\chi^2 = 1713/1415$ dof), and a significant soft excess appears below 1 keV. The addition of a

TABLE 2

RESULTS OF THE FIT IN THE ENERGY RANGE 1.8–100 keV

	PHASE INTERVAL			
PARAMETER	0.1–0.25 (ascent)	0.25–0.35 (maximum)	0.35–0.6 (descent)	0.6–1.1 (minimum)
$N_H(\times 10^{22}$ cm$^{-2})$	1.98 ± 0.05	1.97 ± 0.04	2.00 ± 0.04	2.09 ± 0.04
Photon index	1.244 ± 0.014	1.052 ± 0.020	1.182 ± 0.011	1.462 ± 0.012
E_{cut} (keV)	14.3 ± 0.5	11.35 ± 0.18	$14.08^{+0.08}_{-0.15}$	15.11 ± 0.20
E_{fold} (keV)	8.36 ± 0.9	8.31 ± 0.27	8.76 ± 0.17	6.43 ± 0.17
Smoothing width (keV)	3.9 ± 0.6	4.63 ± 0.17	2.3 ± 0.6	3.7^{+5}_{-4}
Normalization	0.979 ± 0.023	1.21 ± 0.04	0.825 ± 0.017	0.586 ± 0.012
E_{cyc} (keV)	$36.3^{+1.6}_{-2.4}$	31.8 ± 1.1	27.8 ± 0.4	30.6 (fixed)
σ_{cyc} (keV)	$7.4^{+1.7}_{-2.4}$	$9.8^{+2.7}_{-1.9}$	4.8 ± 0.6	5.9 (fixed)
Eye equivalent width (keV)	20 ± 10	26^{+12}_{-8}	11.3 ± 1.6	<8
E_{Fe} (keV)	6.56 ± 0.07	6.50 ± 0.12	6.64 ± 0.06	6.659 ± 0.023
σ_{Fe} (keV)	$0.34^{+0.10}_{-0.05}$	<0.6	0.25 ± 0.08	0.29 ± 0.03
I_{Fe} (photons cm^{-2} s^{-1})	$8.7^{+0.9}_{-1.5} \times 10^{-3}$	$7.0^{+2.8}_{-1.9} \times 10^{-3}$	$(6.4 \pm 1.1) \times 10^{-3}$	$(8.3 \pm 0.5) \times 10^{-3}$
Fe equivalent width (eV)	92	41	73	226
χ^2/dof	291/274	331/274	291/274	308/297

NOTE.—Uncertainties are at the 90% confidence level for a single parameter. Power-law normalizations are in units of 10^{-2} photons keV^{-1} cm^{-2} s^{-1} at 1 keV.

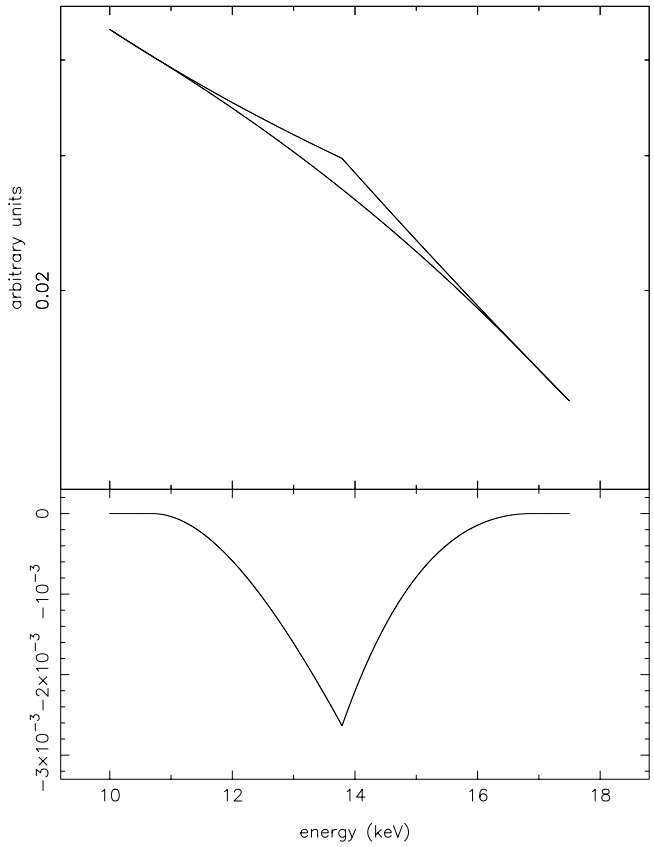

FIG. 5.—*Top*: Plot of the functions $H(E)$ (with a discontinuity in the derivative) and $S(E)$ (smoothed at the cutoff energy). $H(E)$ and $S(E)$ are defined in the text. *Bottom*: Difference $S(E) - H(E)$.

single-temperature blackbody is required at high level of significance ($\Delta\chi^2 = 81$ for two more free parameters), with $kT \simeq 130$ eV, consistent with the *BeppoSAX* result. The absorbtion column density is also consistent with the value obtained by *BeppoSAX*. The spectra and residuals against this best-fit model are shown in Figure 7, while the best-fit parameters are listed in Table 3. The unabsorbed flux in the 0.5–10 keV band is $\simeq 9.0 \times 10^{-10}$ ergs cm^{-2} s^{-1}.

The same model is consistent with the *ROSAT* PSPC outcomes. *ROSAT* observed Cen X-3 on 1992 December

TABLE 3

BEST-FIT PARAMETERS AND RESULTS FOR CONTINUUM MODEL WITH ABSORBED POWER-LAW PLUS THERMAL COMPONENT APPLIED TO *ASCA* AND *ROSAT* DATA

Parameter	*ASCA*	*ROSAT*
$N_{\rm H}(\times 10^{22}$ cm$^{-2})$	$1.54^{+0.13}_{-0.11}$	2.1 ± 0.6
Photon index	$0.64^{+0.05}_{-0.03}$	$1.8^{+0.8}_{-0.5}$
$kT_{\rm BB}$ (eV)	133^{+10}_{-12}	90^{+20}_{-30}
Blackbody normalization.....	$4.2^{+2.9}_{-1.4} \times 10^{-3}$	$0.98^{+5.21}_{-0.96}$
$E_{\rm Fe1}$ (keV)	$6.44^{+0.04}_{-0.02}$	...
$\sigma_{\rm Fe1}$ (eV).....	220^{+80}_{-40}	...
$L_{\rm Fe1}(\times 10^{35}$ ergs s$^{-1})$	$2.2^{+0.4}_{-0.2}$	...
$E_{\rm Fe2}$ (keV)	6.96 (fixed)	...
$\sigma_{\rm Fe2}$ (eV).....	0.0 (fixed)	...
$L_{\rm Fe2}(\times 10^{34}$ ergs s$^{-1})$.....	$3.6^{+2.5}_{-0.9}$	...
χ^2/dof	1632/1413	219.3/186

NOTE.—*ASCA* model also includes a pair of emission lines. The first is broad and takes into account the Kα transitions from Fe I to Fe XXIV. The second is narrow and its centroid energy has been held fixed to 6.96 keV (corresponding to the Kα transition of Fe XXVI).

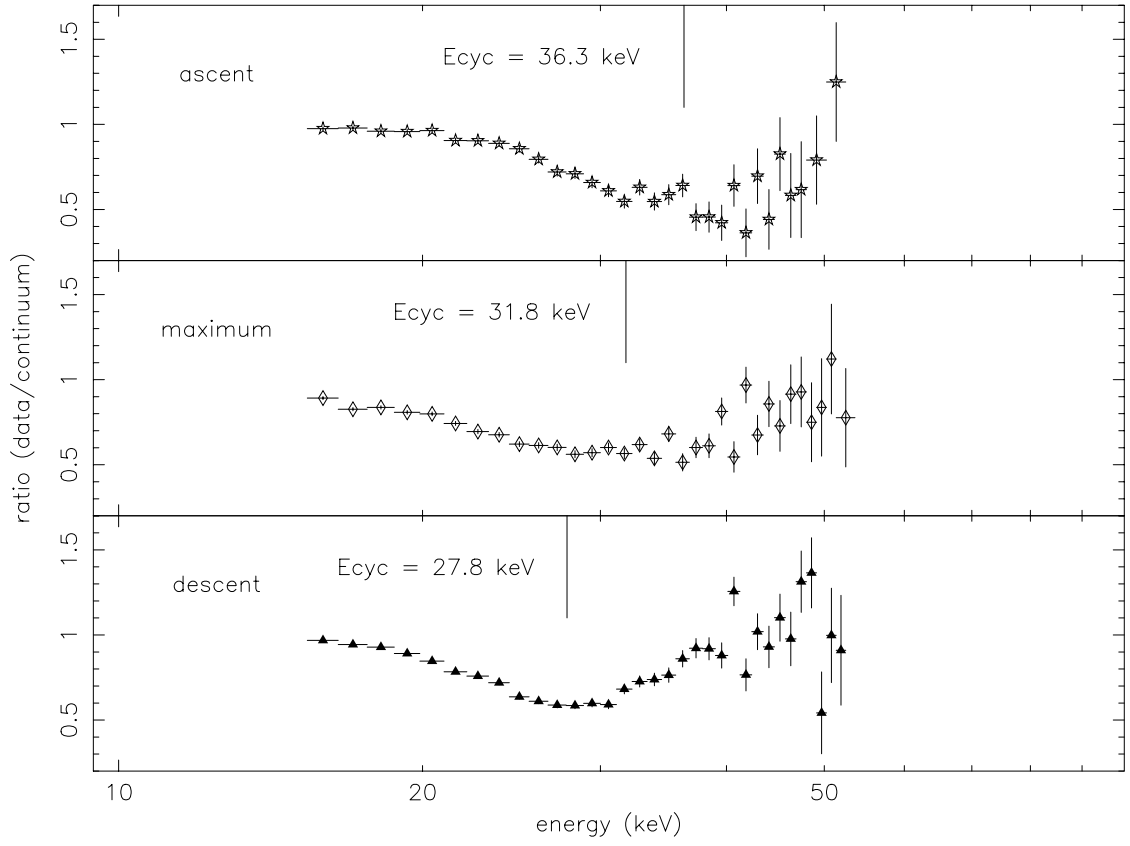

FIG. 6.—Ratio of the total flux over the flux of the continuum (the best-fit model without the cyclotron line) as a function of energy in the phase intervals of ascent, maximum, and descent of the pulse profile (cf. Fig. 2). For each phase interval, the energy of the cyclotron line is also shown.

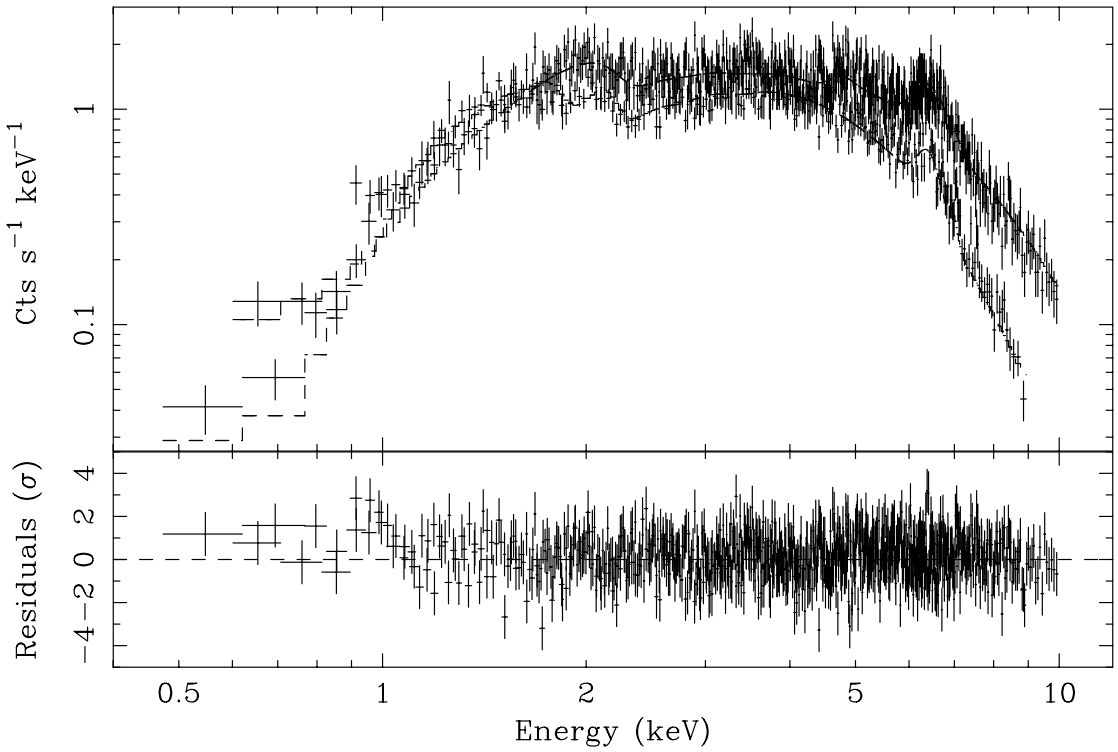

FIG. 7.—Spectra from *ASCA* data and best-fit model (*top*) and residuals in units of standard deviations (*bottom*) with respect to the best-fit model. Only SIS 1 and GIS 3 data are shown, for clarity.

31, from 04:15:20 to 21:47:54 (UTC). We analyzed data corresponding to orbital phases between 0.15 and 0.34. The source spectrum has been extracted from a circular area of 2′ radius around the source centroid, and the background from a concentric annulus between 2.′7 and 4′ from the common center. We considered the energy range 0.1–2 keV, where the response matrix is best calibrated. Although a single-component model does not fit the data (even if

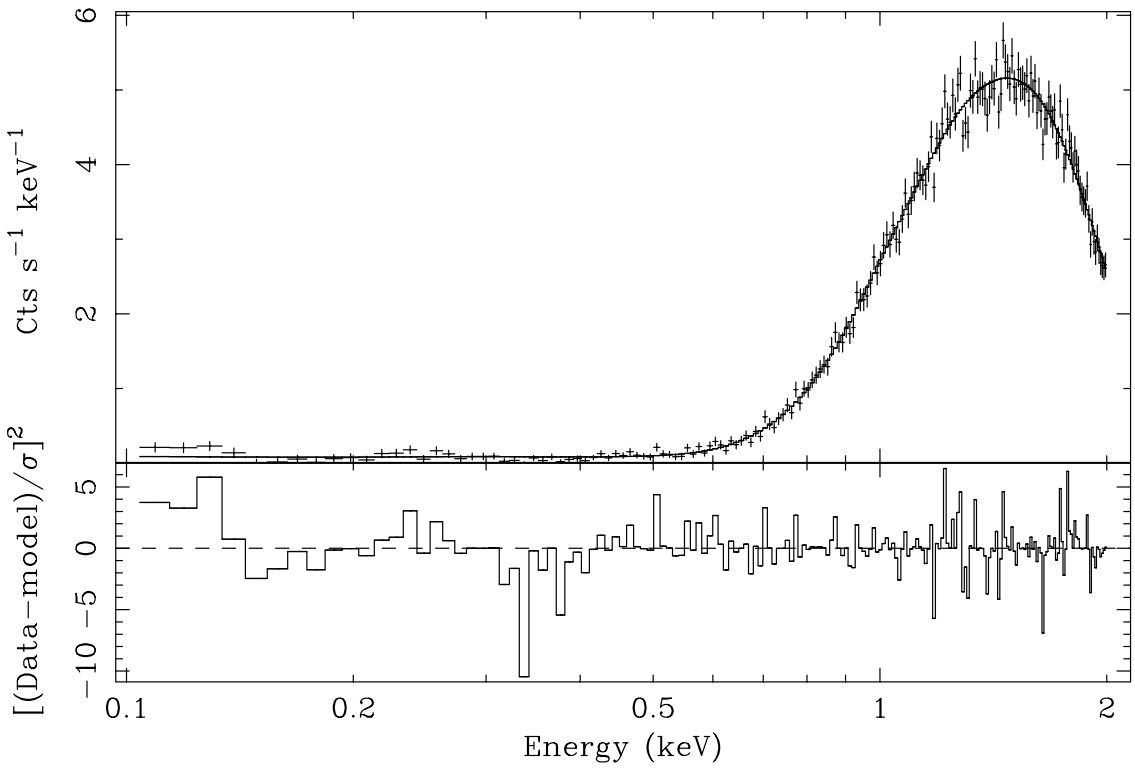

FIG. 8.—Spectra from *ROSAT* PSPC data and best-fit model (*top*) and residuals in units of standard deviations (*bottom*) with respect to the best-fit model.

photoelectric absorption is included), the spectral deconvolution is not unique, and below we discuss only the outcomes of the power-law plus single-temperature thermal component scenario, to compare it with *BeppoSAX* and *ASCA* results. The spectra and residuals against this best-fit model are shown in Figure 8, while the best-fit parameters are listed in Table 3. The quality of the fit is rather good ($\chi^2 = 219.3/186$ dof), the highest residuals being in the 0.2–0.3 keV range, where the PSPC response matrix exhibits a steep gradient and decreases by about 4 orders of magnitude, and still residuals due to calibration uncertainties remain. The absorption column density ($N_{\rm H} \simeq 2 \times 10^{22}$ cm^{-2}) and the temperature of the thermal component ($kT \simeq 90$ eV) are consistent with the results of *BeppoSAX*, as is the poorly determined power-law index. The observed flux in the 0.1–2 keV band is $\simeq 8.4 \times 10^{-11}$ ergs cm^{-2} s^{-1}.

7. DISCUSSION

Here we discuss the main characteristics of the emission of Cen X-3 in the 0.12–100 keV band in order of increasing energy.

The region from 0.1 up to ~ 1 keV is dominated by a blackbody of $kT \sim 0.1$ keV. The unabsorbed flux of this component is 2.2×10^{-8} ergs cm^{-2} s^{-1}, $\sim 58\%$ of the total unabsorbed flux. The corresponding luminosity can be derived from the formula $L_{37} = 0.12 F_{-8}\, d_{\rm kpc}^2$, where L_{37} is the luminosity in units of 10^{37} ergs s^{-1}, F_{-8} is the flux in units of 10^{-8} ergs cm^{-2} s^{-1}, and $d_{\rm kpc}$ is the distance in kpc. Adopting a distance of 8 kpc (Krzemiński 1974), the blackbody luminosity is $L_{\rm BB} = 1.69 \times 10^{38}$ ergs s^{-1}. Since the surface luminosity of a blackbody depends only on its temperature, it is possible to derive the geometrical size of the emitting region, $A = 1.17 \times 10^{12}\, F_{-8}\, d_{\rm kpc}^2\, T_{\rm keV}^{-4}$ cm^2, where $T_{\rm keV}$ is the blackbody temperature in keV. With the above estimates, $A \sim 1.6 \times 10^{18}$ cm^2, which corresponds to a spherical surface of radius $r \sim 3.6 \times 10^8$ cm, comparable to the Alfvén radius. In fact, for an accreting magnetized neutron star, the Alfvén radius, $R_{\rm A}$, is (see, e.g., Burderi et al. 1998)

$$R_{\rm A} = 4.3 \times 10^8\, \mu_{30}^{4/7}\, R_6^{-2/7} L_{37}^{-2/7} \epsilon^{2/7} m^{1/7} \text{ cm}\,, \qquad (2)$$

where μ_{30} is the magnetic moment in units of 10^{30} G cm^3, R_6 is the neutron star radius ($R_{\rm NS}$) in units of 10^6 cm, ϵ is the ratio between the observed luminosity and the total gravitational potential energy released per second by the accreting matter, $\epsilon = L/(GMM/R_{\rm NS})$, and m is the neutron star mass in units of $M_\odot$. Adopting $\mu_{30} = 3.47$ (as deduced from the cyclotron line energy in the hard part of the spectrum; see below), $R_6 = 1$, $m = 1.4$ (typical of a neutron star), $\epsilon \sim 1$, and $L_{37} = 28$ (unabsorbed luminosity), one gets $R_{\rm A} = 3.5 \times 10^8$ cm. The fact that $r \sim R_{\rm A}$ suggests that the Alfvén surface is the blackbody emission region. We stress that the estimate of r is based on the blackbody temperature, while the estimate of $R_{\rm A}$ is based on the magnetic moment strength; therefore, these two quantities are independently estimated. Actually, intense soft emission from X-ray pulsators has been reported for several sources, such as Her X-1 and SMC X-1 (e.g., Holt & McCray 1982; McCray et al. 1982; McCray & Lamb 1976). In particular, McCray & Lamb (1976) suggested that an opaque ringlike shell at the Alfvén radius could surround Her X-1, absorbing a substantial fraction ($\gtrsim 10\%$) of the hard X-ray luminosity and reradiating it as soft X-rays. McCray et al. (1982) estimated that this reprocessor emits as a blackbody with a temperature of ~ 0.1 keV. The fact that $r \sim R_{\rm A}$ and $kT \sim 0.1$ keV for the soft excess of Cen X-3 suggests a similar interpretation. In more detail, the shell has the shape of a spherical ring (i.e., the surface of a sphere minus two opposite spherical caps of equal opening half-angle θ) surrounding the neutron star at the magnetosphere (of radius $r_m = \phi R_{\rm A}$, with $\phi \leq 1$; see below) and lying symmetrically with respect to the accretion disk plane. Therefore, the area of the ring is $A = 4\pi r_m^2 \cos\theta$. We adopted $r_m \sim R_{\rm A}$ and $\theta \sim 65°$, consistent with the estimate of the orbital inclination ($i = 75^\circ {}^{+12^\circ}_{-13^\circ}$; Nagase 1989), in order to have a reprocessor intercepting $\sim 50\%$ of the primary flux that is reemitted as a blackbody (see Fig. 9). In this case, the distance of the reprocessor from the neutron star center is increased by 30% compared to the previous estimate based on a spherical reprocessing surface. We want to stress that reprocessing is a simple way in which a luminosity comparable to the Eddington value can be emitted by a region that is far away from the neutron star surface, where almost all the accretion energy is released.

The region from ~ 1 up to ~ 100 keV is dominated by a power–law continuum with a high-energy cutoff (smoothed at the cutoff energy). This kind of spectrum is typical of X-ray pulsators (White, Nagase, & Parmar 1995) and is interpreted in terms of Comptonization of soft photons by hot electrons of the infalling plasma stopped at the magnetic caps by Coulomb collisions in a strong magnetic field ($\sim 10^{12}$ G; see, e.g., Bulik et al. 1992). In the case of unsaturated Comptonization, the temperature of the electrons can be deduced by the e-fold energy (see, e.g., Rybicki & Lightman 1979). In our case, we have $kT \sim 8$ keV. Mészáros & Nagel (1985a, 1985b) calculated pulse shapes and spectra of X-ray pulsar models adopting slab and column geometry for the emission region (pencil and fan emission, respectively), taking into account self-emitting atmospheres as well as external illumination of the emission region. In the case of self-emitting atmospheres, a low-energy thermal turnover is expected below the electron temperature (~ 8 keV). On the other hand, when an external illumination by soft photons ($kT \sim 0.1$ keV) is considered, there is no thermal turnover at low energies. Indeed, our analysis clearly shows that the spectrum of Cen X-3 matches this second model. In this latter case, the luminosity in X-rays is generated by hot electrons ($kT \sim 8$ keV) heated by the accretion process, upscattering seed soft photons ($kT \sim 0.1$ keV) that are provided by a different source. The calculations show that, for this model to work, the flux of soft photons incident on the hot electrons must be enhanced (up to 10^4 times) with respect to the number of photons expected from a blackbody of 0.1 keV and an emitting surface of 10 km^2, typical for a polar cap. A possible production mechanism for such a copious quantity of soft photons is the resonant (at cyclotron energy) double photon scattering, as originally proposed by Bussard, Mészáros, & Alexander (1985), although their calculations gave a production rate of soft photons a factor of 5 less than the number needed. Alternatively, based on the soft excess discussed above, we suggest that the soft photons could come from the reprocessor at the magnetosphere, which has the correct blackbody temperature and an emitting area larger than the neutron star surface, capable of furnishing a higher quantity of photons. In the first approximation, the fraction of soft photons intercepted by the neutron star is $(R_{\rm NS}/r_m)^2$.

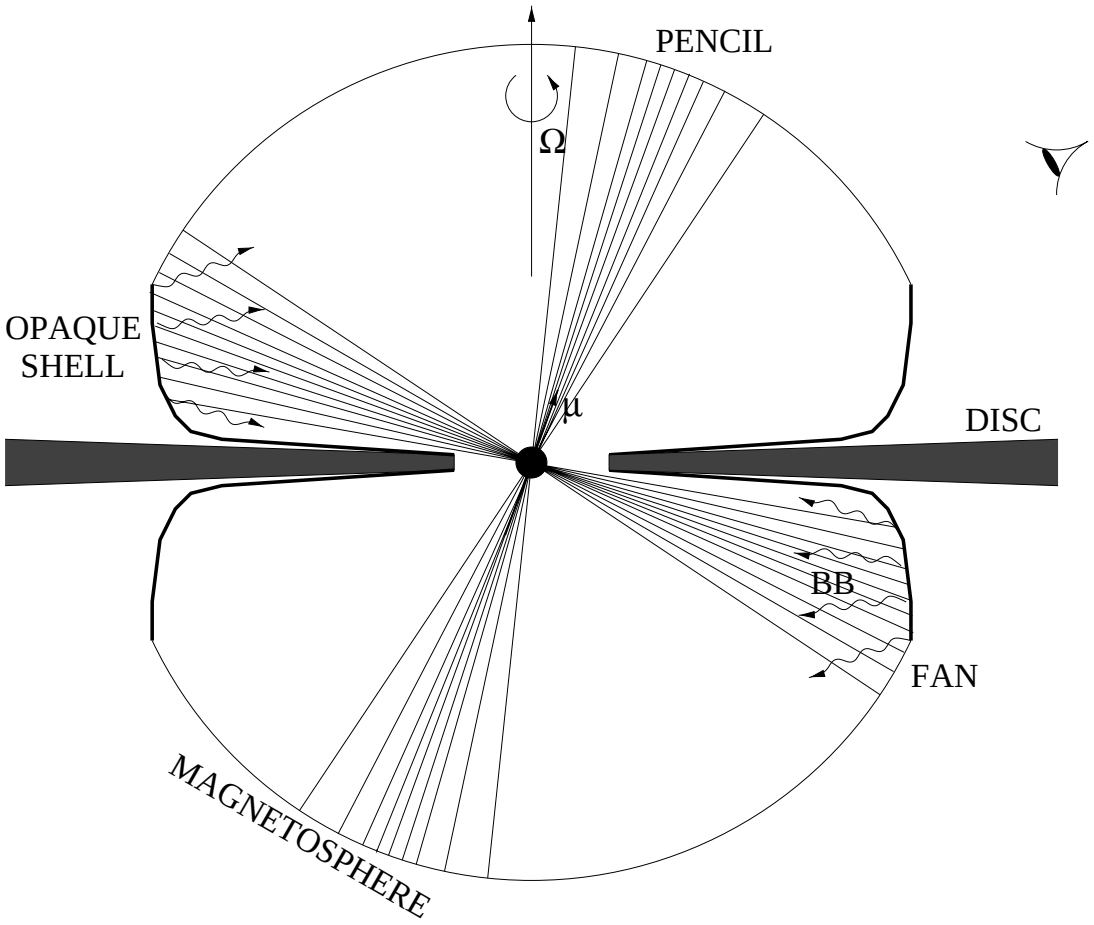

FIG. 9.—Schematic model of the emission region of Cen X-3. The inclination angle of the line of sight is 65°, within the range given by Nagase (1989). The inclination of the magnetic dipole is 20°, in order to have a single-peaked pulse profile. The Comptonized emission (hard component) comes from the pencil beam. The fan beam intercepts the opaque shell at the magnetosphere originating the soft component. The fraction of the fan beam not intercepted by the opaque shell might be responsible for the secondary peak of the pulse profile.

Therefore, the energy per unit time incident on the polar cap is $L_{\rm BB} \times (R_{\rm NS}/r_m)^2 \sim 10^{34}$ ergs s^{-1}. This is an order of magnitude below the luminosity of the soft component adopted by Mészáros & Nagel (1985a, 1985b). This discrepancy can be reduced if, as shown in Figure 9, the accretion disk significantly distorts the shape of the magnetosphere (Ghosh & Lamb 1991), reducing the magnetospheric radius r_m, to the value $\phi R_{\rm A}$, where ϕ is in the range 0.1–0.5 (see, e.g., Ghosh & Lamb 1991; Burderi et al. 1998). This raises the luminosity of the soft component up to 4×10^{34}–10^{36} ergs s^{-1}.

Since in our model the soft photons originate from a reprocessing of the primary radiation, which in turn results from upscattering of the soft photons (namely, the cooling of the electrons of the accreting plasma), a feedback mechanism is driving the whole process. This feedback process is similar to the model proposed to explain the power-law spectra of accreting black holes (e.g. Dove et al. 1997). However, in the black hole case, the mechanism that keeps the temperature of the corona at $\sim$100 keV is not clear, while electron temperatures of $\sim$10 keV are expected for a plasma decelerated by Coulomb collisions on the surface of a neutron star. If this interpretation is correct, we expect that the spectrum of this kind of source is a power law extending down to the soft X-ray range plus a thermal component, when the feedback cooling mechanism proposed above is active through a reprocessing process. On the other hand, when the reprocessor is absent or the geometry of the emission region is such that the beam does not intercept it, a low-energy turnover is expected in the power law below the electron temperature (a few keV).

An absorption feature at energies $\sim$30.6 keV is clearly detected on this continuum. The feature is well fitted by a Gaussian profile of $\sigma \sim 5.9$ keV. We interpreted this line as due to resonant absorption at the cyclotron energy. To obtain the strength of the magnetic field, we considered the relation between the cyclotron energy and the magnetic field, $E_{\rm cycl}/(1\ {\rm keV}) = 11.6B/(10^{12}\ {\rm G})$. We also considered that the gravitational redshift at the neutron star surface affects the observed energy, $E_{\rm cycl} = E_{\rm obs}(1 + z)$, where $(1 + z) = (1 - 2GM_{\rm NS}/Rc^2)^{-1/2}$ is the redshift factor. Adopting a standard neutron star mass of 1.4 $M_\odot$, we found $E_{\rm c} = 40.3$ keV and a magnetic field strength of $B = 3.47 \times 10^{12}$ G. This is in excellent agreement with the estimate of $B = 3.4 \times 10^{12}$ G derived by Audley et al. (1996) assuming that during the QPO episode observed by BBXRT the neutron star was spinning up.

An estimate of the temperature of the region in which the cyclotron line is formed can be deduced from the width of the line itself. If the electrons have a temperature kT, the Doppler broadening of the line is given by $\Delta E/E_{\rm c} = (2kT/m_{\rm e}c^2)^{1/2}$ (see, e.g., Rybicki & Lightman 1979).

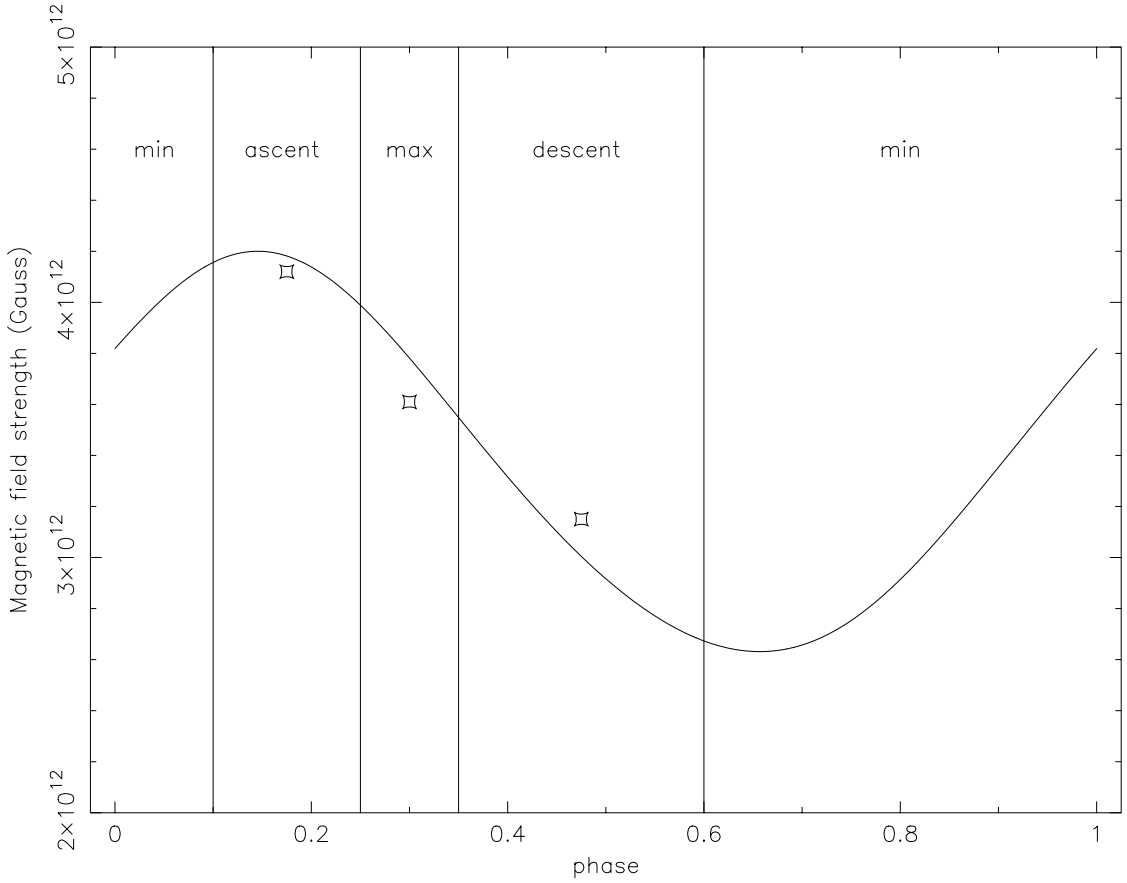

FIG. 10.—Solid line represents the magnetic field strength as a function of the pulse phase for a magnetic dipole offset by 0.1 R_{NS} with respect to the center of the neutron star. The data points are the measured magnetic field strength as derived from pulse-phase–resolved spectral analysis. Typical errors on the estimate of the magnetic field strength are $\pm 0.15 \times 10^{12}$ G. The intervals refers to the pulse shape shown in Fig. 2*c*.

Adopting the values of the detected absorption feature, we obtained $kT = 9.5$ keV. This important result provides a self consistency check for the interpretation of the whole spectrum. In fact, the temperature of the plasma derived from the high-energy rollover is, within the errors, perfectly consistent with that derived from the thermal broadening of the line.

We used a Gaussian profile to describe the cyclotron absorption line instead of the widely used pseudo-Lorentzian shape (Mihara 1995). We believe that a Gaussian profile should be used whenever thermal Doppler broadening is dominant. Actually, the Compton cross section in a magnetized cold plasma for the scattering $1 \rightarrow 1$ (from extraordinary mode to extraordinary mode) has the shape $\sigma(E) = \sigma_T E^2/[(E - E_{cycl})^2 + W^2]$, where σ_T is the Thomson cross section and W is the width of the resonance (Ventura 1979). The natural width of the resonance is ~ 10 eV (Nagel 1980). The line profile results from the convolution of the above cross section with a relativistic Maxwellian distribution of velocities (Synge 1957). Performing the convolution, because the gas temperature (~ 8 keV) is much greater than the natural width, one finds that a Gaussian is an excellent approximation of the line profile.

As discussed above, the phase-resolved spectra show a strong dependence of the energy of the absorption feature at ~ 30 keV along the pulse profile. In principle, small variations (< 1 keV) of the line energy with the angle between the magnetic axis and the line of sight are expected (Mészáros & Nagel 1985a, 1985b). In this case, the expected variations of the cyclotron line energy are symmetric with respect to the peak of the pulse profile. On the other hand, we found variations in the line energy up to 8 keV that are asymmetric along the pulse profile. In particular, the line energy decreases along the peak starting from the ascent. Because of the dependence of the dipolar magnetic field on the angle between the magnetic axis and the line of sight (χ) and on the distance from the center, variations of the cyclotron energy along with the pulse phase might be caused by the variation of χ and/or of the height of the accretion column over the polar cap. However, these effects can hardly explain the asymmetric variation of the cyclotron energy with the pulse phase. In principle, a wide polar cap (with an opening angle of about 50°–60°) could give variations of the cyclotron energy of the order of magnitude of those observed ($\sim 30\%$), but we expect these to be symmetric with respect the magnetic axis (and therefore the pulse profile). Similar variations can also be produced by a gradient in the height of the line formation region along the accretion column. In this case, we should have a difference in the height of the formation region of $\sim 10\%$–15% of the neutron star radius from one side of the accretion column to the other. However, it is unlikely to have variations of the physical parameters capable of giving a difference of about 1 km in the height of the formation region from one side of the accretion column to the other. This asymmetric behavior can be more easily explained by assuming that

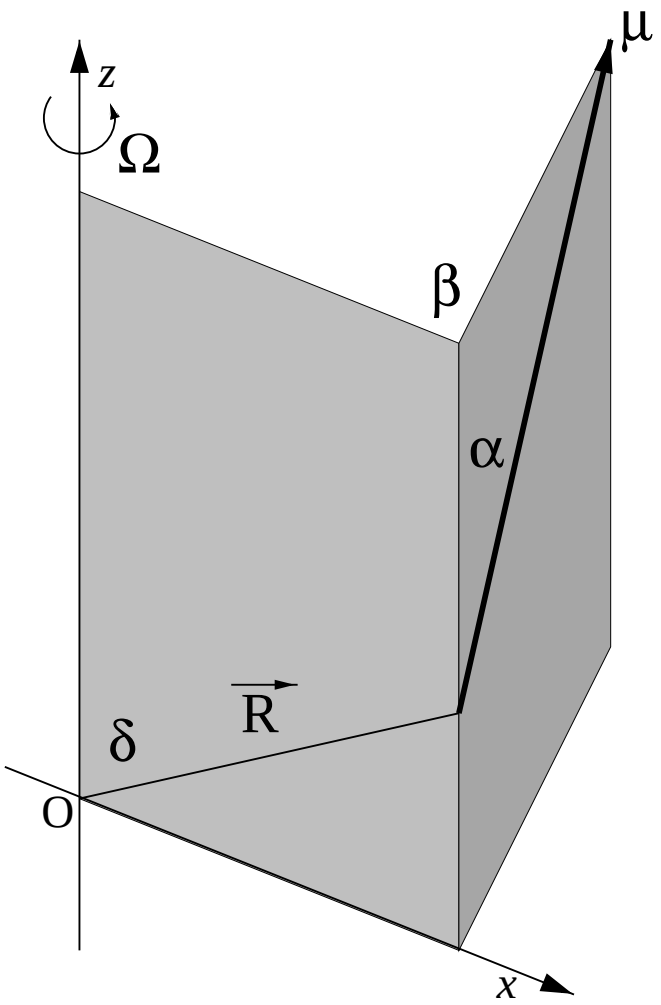

FIG. 11.—Geometry of the magnetic moment with respect to the center of the neutron star and the rotation axis. O is the neutron star center, the z-axis is the rotation axis, $\boldsymbol{R}$ is the offset vector of modulus 0.1 R_{NS}, $\delta = 80°$ is the angle of $\boldsymbol{R}$ with respect to the z-axis, μ is the magnetic moment, $\alpha = 20°$ is the inclination angle of μ with respect to the spin axis, and $\beta = 130°$ is the angle between the plane of the magnetic moment and the plane of the offset vector.

the center of the magnetic dipole is offset with respect to the neutron star center. In this case, the strength of the surface magnetic field decreases along the magnetic cap originating the observed asymmetric line variations. Offset magnetic moments are expected to be present in X-ray pulsators, as proposed by Leahy (1991) from a geometrical analysis of the pulse profile of several sources; in particular, Cen X-3 is expected to have a significant offset of the magnetic dipole. To demonstrate how this works, in Figure 10 we plot the surface magnetic dipole strength at a fixed latitude (corresponding to the expected inclination of the line of sight with respect to the spin axis of the neutron star) along the pulse phase for a magnetic dipole inclined (20°) with respect to the spin axis and displaced (by 0.1 R_{NS}) with respect to the neutron star center. The location and orientation of the magnetic dipole are described in Figure 11. As it is possible to observe in Figure 10, the agreement between the field strength variations predicted by the offset dipole model and the results of the pulse-phase–resolved spectral analysis (Table 2) is very good.

To summarize, the points discussed above suggest the model sketched in Figure 9. The emission is probably a mixture of fan and pencil. The fan beam intercepts the opaque shell at the magnetosphere originating the reprocessed soft component. On the other hand, the pencil beam is not blocked by the shell and is responsible for the Comptonized emission (hard component). In this way, the hard and soft components pulse in phase; moreover, the fraction of the fan beam not intercepted by the opaque shell originates the secondary peak of the pulse profile at 180° from the main peak. The inclination angle of the line of sight is 65°, in the range given by Nagase (1989), based on the eclipse. The inclination of the magnetic dipole is 20°, which satisfies the constraint given by Wang & Welter (1981) in order to have a single peak, as observed.

8. CONCLUSIONS

We analyzed *BeppoSAX* data in the high post-egress state of the X-ray pulsator Centaurus X-3. The *BeppoSAX* broadband spectrum (0.1–100 keV) is well fitted by an absorbed power-law continuum (photon index ~ 1.2) modified by a high-energy rollover (cutoff energy ~ 14 keV, e-folding energy ~ 8 keV) smoothed around the cutoff energy. A soft feature at ~ 1 keV is well fitted by a blackbody of $kT \sim 0.1$ keV, with a total unabsorbed flux that is $\sim 50\%$ of the total emission. Both the *ASCA* and the *ROSAT* out-of-eclipse spectra confirm the presence of a soft X-ray thermal component of $kT \sim 0.1$ keV. We interpret this component in terms of the reprocessing of the primary radiation by an opaque shell at the magnetosphere. The fraction of the reprocessed flux intercepted by the polar cap could be the source of soft photons needed to originate the (Comptonized) primary radiation. This feedback mechanism can efficiently cool the electrons of the accreting matter, originating a power law extending to the soft X-rays. On the other hand, for sources in which the reprocessing process is uneffective, we predict a low-energy turnover in the primary spectrum below the electron temperature (a few keV). Further analyses of the soft region of the spectrum of X-ray pulsators are needed to confirm this model.

An absorption feature at ~ 30 keV is well described by cyclotron absorption from the surface magnetic field at the polar cap. The derived magnetic field intensity of 3.47×10^{12} G is consistent with previous independent estimates. Phase-resolved spectroscopy shows that the line energy is decreasing along the pulse peak from ~ 36 keV at the ascent down to ~ 28 keV at the descent. This behavior can be explained by an offset of the magnetic dipole with respect to the neutron star center.

This work was supported by the Italian Space Agency (ASI), and by the Ministero della Ricerca Scientifica e Tecnologica (MURST).

REFERENCES

Audley, M. D., et al. 1996, ApJ, 457, 397
Boella, G., Butler, R. C., Perola, G. C., Piro, L., Scarsi, L., & Blecker, J. 1997a, A&AS, 122, 299
Boella, G., Chiappetti, L., Conti, G., Cusumano, G., Del Sordo, S., La Rosa, G., Maccarrone, M. C., Mineo, T., Molendi, S., Re, S., Sacco, B., & Tripiciano, M. 1997b, A&AS, 122, 327
Bulik, T., Mészáros, P., Woo, J. W., Nagase, F., & Makishima, K. 1992, ApJ, 395, 564
Burderi, L., Di Salvo, T., Robba, N. R., Del Sordo, S.,Santangelo, A., & Segreto, A. 1998, ApJ, 498, 831
Bussard, R. W., Mészáros, P., & Alexander, S. 1985, ApJ, 297, L21
Dove, J. B., Wilms, J., Maisack, M., & Begelman, M. 1997, ApJ, 487, 759
Frontera, F., Costa, E., Dal Fiume, F., Feroci, M., Nicastro, L., Orlandini, M., Palazzi, E., & Zavattini, G. 1997, A&AS, 122, 357
Ghosh, P., & Lamb, F. K. 1991, in Neutron Stars: Theory and Observation, ed. J. Ventura & D. Pines (Nato ASI Ser. C, 344; Dordrecht: Kluwer), 363
Hiroshi, T., Kitamoto, S., & Tamura, K. 1996, ApJ, 456, 316
Holt, S. S., & McCray, R. 1982, ARA&A, 20, 323
Hutchings, J. B., Cowley, A. P., Crampton, D., van Paradijs, J., & White, N. E. 1979, ApJ, 229, 1079
Krzemiński, W. 1974, ApJ, 192, L135
Leahy, D. A. 1991, MNRAS, 251, 203
Makishima, K., et al. 1996, PASJ, 48, 17
Manzo, G., Giarrusso, S., Santangelo, A., Ciralli, F., Fazio, G., Piraino, S., & Segreto, A. 1997, A&AS, 122, 341
McCray, R., & Lamb, F. K. 1976, ApJ, 204, L115
McCray, R., Shull, J. M., Boynton, P. E., Deeter, J. E., Holt, S. S., & White, N. E. 1982, ApJ, 261, 301
Mészáros, P., & Nagel, W. 1985a, ApJ, 298, 147
———. 1985b, ApJ, 299, 138
Mihara, T. 1995, Ph.D. thesis, Univ. Tokyo
Nagase, F. 1989, PASJ, 41, 1
Nagase, F., Corbet, R. H. D., Day, C. S. R., Inoue, H., Takeshima, T., Yoshida, K., & Mihara, T. 1992, ApJ, 396, 147
Nagel, W. 1980, ApJ, 236, 904
Parmar, A. N., Martin, D. D. E., Bavdaz, M., Favata, F., Kuulkers, E., Vacanti, G., Lammers, U., Peacock, A., & Taylor, B. G. 1997, A&AS, 122, 309
Priedhorsky, W. C., & Terrell, J. 1983, ApJ, 273, 709
Rybicki, G. R., & Lightman, A. P. 1979, Radiative Processes in Astrophysics (New York: Wiley)
Santangelo, A., Del Sordo, S., Segreto, A., Dal Fiume, D., Orlandini, M., & Piraino, S. 1998, A&A, 340, L55
Synge, J. L. 1957, The Relativistic Gas (Amsterdam: North-Holland)
Tanaka, Y., Inoue, H., & Holt, S. S. 1994, PASJ, 46, L37
van der Klis, M., Bonnet-Bidaud, J. M., & Robba, N. R. 1980, A&A, 88, 8
Ventura, J. 1979, Phys. Rev. D, 19, 1684
Wang, Y.-M., & Welter, G. L. 1981, A&A, 102, 97
White, N. E., Nagase, F., & Parmar, A. N. 1995, in X-Ray Binaries, ed. W. H. G. Lewin, J. van Paradijs, & E. P. J van den Heuvel (Cambridge: Cambridge Univ. Press), 1
White, N. E., Swank, J. H., & Holt, S. S. 1983, ApJ, 270, 711